

DeepSplit: Scalable Verification of Deep Neural Networks via Operator Splitting

Shaoru Chen^{*}, Eric Wong[†], J. Zico Kolter[‡], Mahyar Fazlyab^{§¶}

Abstract

Analyzing the worst-case performance of deep neural networks against input perturbations amounts to solving a large-scale non-convex optimization problem, for which several past works have proposed convex relaxations as a promising alternative. However, even for reasonably-sized neural networks, these relaxations are not tractable, and so must be replaced by even weaker relaxations in practice. In this work, we propose a novel operator splitting method that can directly solve a convex relaxation of the problem to high accuracy, by splitting it into smaller sub-problems that often have analytical solutions. The method is modular and scales to problem instances that were previously impossible to solve exactly due to their size. Furthermore, the solver operations are amenable to fast parallelization with GPU acceleration. We demonstrate our method in obtaining tighter bounds on the worst-case performance of large convolutional networks in image classification and reinforcement learning settings.

1 Introduction

Despite their superior performance, neural networks lack formal guarantees, raising serious concerns about their adoption in safety-critical applications such as autonomous vehicles [4] and medical machine learning [14]. Motivated by this drawback, there has been an increasing interest in developing tools to verify desirable properties for neural networks, such as robustness to adversarial attacks. Neural network verification refers to the problem of verifying whether the output of a neural network satisfies certain properties for a bounded set of input perturbations. This problem can be framed as optimization problems of the form

$$\text{minimize } J(f(x)) \quad \text{subject to } x \in \mathcal{X}, \quad (1)$$

where f is given by a deep neural network, J is a real-valued function representing a performance measure (or a specification), and \mathcal{X} is a set of inputs to be verified. In this formulation, verifying the neural network amounts to certifying whether the optimal value of (1) is bounded below by a certain threshold. This problem is large-scale and non-convex, making it extremely difficult to solve efficiently—both in terms of time and memory. For ReLU activation functions and linear objectives, the problem in (1) can be cast as a Mixed-Integer Linear Program (MILP) [5, 9, 15, 22], which can

^{*}Department of Electrical and Systems Engineering, University of Pennsylvania, email: srchen@seas.upenn.edu

[†]Computer Science and Artificial Intelligence Laboratory, Massachusetts Institute of Technology, email: wongeric@mit.edu

[‡]Computer Science Department, Carnegie Mellon University, email: zkolter@cs.cmu.edu

[§]Department of Electrical and Computer Engineering and Mathematical Institute for Data Science, Johns Hopkins University, email: mahyarfazlyab@jhu.edu

[¶]Shaoru Chen and Eric Wong contributed equally.

Corresponding Author: Mahyar Fazlyab email: mahyarfazlyab@jhu.edu

be solved for the global solution via, for example, branch-and-bound methods. While we do not expect these approaches to scale to large problems, for small neural networks they can still be practical.

Instead of solving (1) for its global minimum, one can instead find *guaranteed lower bounds* on the optimal value via convex relaxations, such as Linear Programming (LP) [36] and Semidefinite Programming (SDP) [12, 13, 27]. Verification methods based on convex relaxations are sound but incomplete, i.e., they are guaranteed to detect all false negatives but also produce false positives, whose rate depends on the tightness of the relaxation. Although convex relaxations are polynomial-time solvable, in practice they are not computationally tractable for large-scale neural networks. To improve scalability, these relaxations must typically be further relaxed [2, 10, 35, 36, 43].

Contributions. In this work, we propose an algorithm for solving convex relaxations *exactly* for large-scale neural networks. Our starting point is to express (1) as a constrained optimization problem whose constraints are imposed by the forward passes in the network. We then introduce additional decision variables and consensus constraints that naturally split the corresponding problem into independent subproblems, which often have closed-form solutions. Finally, we employ an operator splitting technique based on the alternating direction method of multipliers (ADMM) [1], to solve the corresponding Lagrangian relaxation of the problem. This approach has several favorable properties. First, the method requires minimal parameter tuning and relies on simple operations, which scale to very large problems and can achieve a good trade-off between runtime and solution accuracy. Second, all the solver operations are amenable to fast parallelization with GPU acceleration. Third, our method is fully modular and applies to standard network architectures.

We employ our method to compute exact solutions to LP relaxations on the worst-case performance of adversarially trained deep networks, with a focus on networks that were previously impossible to solve exactly to due to their size. Specifically, we perform extensive experiments in the ℓ_∞ perturbation setting, where we verify robustness properties of image classifiers in MNIST and CIFAR10, and deep Q-networks (DQNs) in Atari games [42]. Our method is able to quickly solve LP relaxations at scales that are too large for tighter bounds such as SDP relaxations or commercial LP solvers such as Gurobi, and provide speedups over Gurobi at smaller scales.

1.1 Related Work

Convex relaxations LP relaxations are relatively the most tractable form of convex relaxations [11]. However, even solving LPs can become computationally prohibitive for small convolutional networks [28]. One line of work studies computationally cheaper but looser bounds of the LP relaxation [36], which have been extended to more general networks and settings [35, 38, 39, 43]. These bounds tend to be loose unless optimized during training, which typically comes at a significant cost to standard performance. Further work has aimed to tighten these bounds [7, 31, 33], however these works focus primarily on small convolutional networks and struggle to scale to more typical deep networks. Other work has studied the limits of these convex relaxations on these small networks using vast amounts of CPU-compute [28]. Recent SDP-based approaches [6] can produce much tighter bounds on these small networks, rendering most LP-based approaches obsolete in the small-network regime.

Lagrangian-based bounds Most related to our work is that which solves the Lagrangian of the LP relaxation [2, 10], which can tighten the bound but do not aim to solve the LP exactly due to poor convergence. However, these works primarily study small networks whose LP relaxation can still be solved exactly with Gurobi, and the resulting bounds are superseded by SDP-based bounds that can scale to these networks [6]. Although these works could in theory be used on larger networks,

only the faster, linear-based bounds [39] have demonstrated applicability to standard deep learning architectures. In our work, we solve the LP relaxation exactly in *large* network settings that, up to this point, have only been studied with loose bounds of the LP relaxation such as LiRPA [39].

Complete verification methods Complete verifiers attempt to verify properties of deep networks exactly using methods such as SMT solvers [20, 29] and MILP solvers [5, 9, 15, 22]. A common strategy is to use the LP relaxation to compute cheaper, intermediate bounds to greatly speed up their practical running time [3, 11, 34]. In particular, MILP solvers using branch-and-bound or cutting planes rely on solving a sequence of LP relaxations as a subroutine to find the global solution. However, exactly solving the LP relaxation remains a major bottleneck for large networks. Our work addresses this bottleneck and allows for the computation of tighter intermediate bounds for large neural networks that were previously computationally intractable.

Operator splitting methods Operator splitting, and in particular the ADMM method, is a powerful technique in solving structured convex optimization problems and has applications in numerous settings ranging from optimal control [26] to training neural networks [32]. These methods scale well with the problem dimensions, can exploit sparsity in the problem data efficiently [45], are amenable to parallelization on GPU [30], and have well-understood convergence properties under minimal regularity assumptions [1]. The benefit of ADMM as an alternative to interior-point solvers has been shown in various classes of optimization problems [25]. Our operator splitting method is specifically tailored for neural network verification in order to fully exploit the problem structure.

Notation. We denote the set of real numbers by \mathbb{R} , the set of nonnegative real numbers by \mathbb{R}_+ , the set of real n -dimensional vectors by \mathbb{R}^n , the set of $m \times n$ -dimensional matrices by $\mathbb{R}^{m \times n}$, and the n -dimensional identity matrix by I_n . The p -norm ($p \geq 1$) is denoted by $\|\cdot\|_p: \mathbb{R}^n \rightarrow \mathbb{R}_+$. For a set \mathcal{S} , we define the indicator function $\mathbb{I}_{\mathcal{S}}(x)$ of \mathcal{S} as $\mathbb{I}_{\mathcal{S}}(x) = 0$ if $x \in \mathcal{S}$ and $\mathbb{I}_{\mathcal{S}}(x) = \infty$ otherwise. Given a function $f: \mathcal{X} \rightarrow \mathcal{Y}$, the graph of f is the set $\mathcal{G}_f = \{(x, f(x)) \mid x \in \mathcal{X}\}$.

2 Scalable Neural Network Verification via Operator Splitting

We consider an ℓ -layer feed-forward neural network $f(x): \mathbb{R}^{n_0} \rightarrow \mathbb{R}^{n_\ell}$ described by the following recursive equations,

$$x_0 = x, \quad x_{k+1} = \phi_k(x_k) \quad k = 0, \dots, \ell - 1, \quad f(x) = x_\ell \quad (2)$$

where $x_0 \in \mathbb{R}^{n_0}$ is the input to the neural network, $x_k \in \mathbb{R}^{n_k}$ is the input to the k -th layer, and $\phi_k: \mathbb{R}^{n_k} \rightarrow \mathbb{R}^{n_{k+1}}$ is the operator of the k -th layer, which can represent any commonly-used operator in deep networks, such as linear (convolutional) layers, MaxPooling units, and activation functions.

Given the neural network f , a specification function $J: \mathbb{R}^{n_\ell} \mapsto \mathbb{R}$, and an input set $\mathcal{X} \subset \mathbb{R}^{n_0}$, we say that f satisfies the specification J if $J(f(x)) \geq 0$ for all $x \in \mathcal{X}$. This is equivalent to verifying that the optimal value of (1) is non-negative. We assume $\mathcal{X} \subset \mathbb{R}^{n_0}$ is a closed convex set and $J: \mathbb{R}^{n_\ell} \rightarrow \mathbb{R} \cup \{+\infty\}$ is a convex function, defining a performance measure on the output of the network. Note that our formulation generalizes to arbitrary computational graphs (e.g. residual blocks) and general objective functions (see Appendix A).

Using the sequential representation of the neural network in (2), we may rewrite the optimization problem in (1) as the following constrained optimization problem,

$$p^* \leftarrow \text{minimize} \quad J(x_\ell) \quad \text{subject to} \quad x_{k+1} = \phi_k(x_k), \quad k = 0, \dots, \ell - 1, \quad x_0 \in \mathcal{X}, \quad (3)$$

Algorithm 1: DeepSplit Algorithm

Data: Neural network f (Eq. 2), bounded convex input set \mathcal{X} , convex function J .

Initialization: $x_0 \in \mathcal{X}$, $x_{k+1} = \phi_k(x_k)$, $y_k = x_k$, $z_k = x_{k+1}$, $\lambda_k = 0$, $\mu_k = 0$,
 $k = 0, \dots, \ell - 1$, augmentation constant $\rho > 0$.

repeat

Step 1: x-update (9)

Step 2: (y, z)-update (10)

Step 3: dual update (13)

until *stopping criterion is met*;

Output: $J(x_\ell)$

with $n := \sum_{k=0}^{\ell} n_k$ decision variables. We can rewrite (3) equivalently as

$$p^* \leftarrow \text{minimize } J(x_\ell) \quad \text{subject to } (x_k, x_{k+1}) \in \mathcal{G}_{\phi_k}, \quad k = 0, \dots, \ell - 1, \quad x_0 \in \mathcal{X}, \quad (4)$$

where $\mathcal{G}_{\phi_k} = \{(x_k, x_{k+1}) \mid x_{k+1} = \phi_k(x_k), \underline{x}_k \leq x_k \leq \bar{x}_k\}$ is the graph of ϕ_k . This problem is non-convex due to presence of nonlinear operators in the network, such as activation layers. By over-approximating \mathcal{G}_{ϕ_k} by a convex set (or ideally by its convex hull), we arrive at a direct layer-wise convex relaxation of the problem. However, this relaxation cannot scale to even medium-sized neural networks. In this section, by exploiting the sequential structure of the constraints, we propose a reformulation of (3) whose convex relaxation can be solved efficiently and in a scalable manner.

2.1 Variable Splitting

By introducing the intermediate variables y_k and z_k , we can rewrite (3) as

$$\begin{aligned} p^* \leftarrow \text{minimize} \quad & J(x_\ell) & (5) \\ \text{subject to} \quad & y_k = x_k & k = 0, \dots, \ell - 1 \\ & z_k = \phi_k(y_k) & k = 0, \dots, \ell - 1 \\ & x_{k+1} = z_k & k = 0, \dots, \ell - 1 \\ & x_0 \in \mathcal{X} \end{aligned}$$

which has now $2n - n_0 - n_\ell$ decision variables. Intuitively, we have introduced additional “identity layers” between consecutive layers (see Figure 1). By overapproximating \mathcal{G}_{ϕ_k} by a convex set \mathcal{S}_{ϕ_k} , we obtain the convex relaxation

$$\begin{aligned} p_{\text{relaxed}}^* \leftarrow \text{minimize} \quad & J(x_\ell) & (6) \\ \text{subject to} \quad & y_k = x_k & k = 0, \dots, \ell - 1 \\ & (y_k, z_k) \in \mathcal{S}_{\phi_k} & k = 0, \dots, \ell - 1 \\ & x_{k+1} = z_k & k = 0, \dots, \ell - 1 \\ & x_0 \in \mathcal{X}, \end{aligned}$$

for which $p_{\text{relaxed}}^* \leq p^*$. This form is known as consensus as y_k and z_{k-1} are just copies of the variable x_k . As shown below, this “overparameterization” allows us to split the optimization problem into smaller sub-problems across layers that can be solved in parallel and often in closed form.

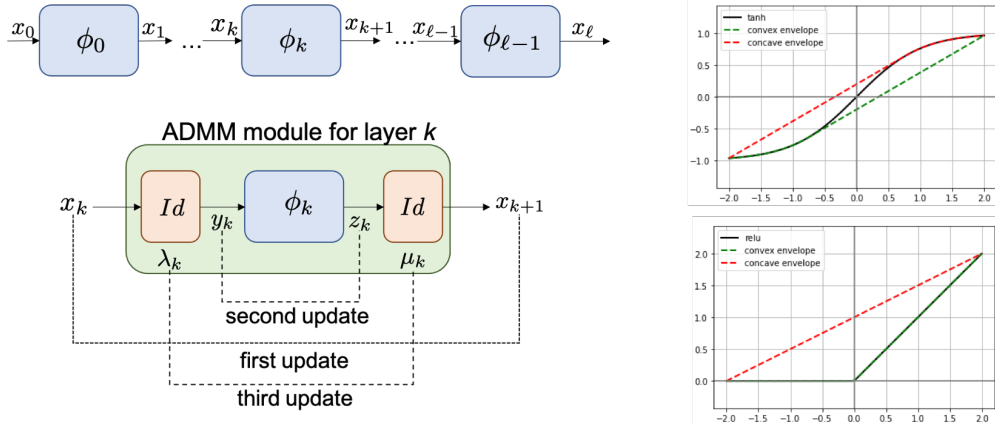


Figure 1: Left: Illustration of the network structure (Top) and the DeepSplit computation module for a generic layer (Bottom). Adding identity layers in between the neural network layers decouples the variables x_k and allows processing them independently. Right: Over-approximation of the graph of ReLU (Top) and tanh (Bottom) function by their convex hull.

2.2 Lagrangian Relaxation and Operator Splitting

We use $\mathbf{x} = (x_0, \dots, x_\ell)$, $\mathbf{y} = (y_0, \dots, y_{\ell-1})$ and $\mathbf{z} = (z_0, \dots, z_{\ell-1})$ to denote the concatenated variables. By relaxing the equality constraints with Lagrangian multipliers, we define the augmented Lagrangian for (6) as follows,

$$\begin{aligned} \mathcal{L}(\mathbf{x}, \mathbf{y}, \mathbf{z}, \boldsymbol{\lambda}, \boldsymbol{\mu}) = & J(x_\ell) + \sum_{k=0}^{\ell-1} \mathbb{I}_{\mathcal{S}_{\phi_k}}(y_k, z_k) + \mathbb{I}(x_0 \in \mathcal{X}) + (\rho/2) \sum_{k=0}^{\ell-1} (\|x_k - y_k + \lambda_k\|_2^2 - \|\lambda_k\|_2^2) \\ & + (\rho/2) \sum_{k=0}^{\ell-1} (\|x_{k+1} - z_k + \mu_k\|_2^2 - \|\mu_k\|_2^2). \end{aligned} \quad (7)$$

where $\boldsymbol{\lambda} = (\lambda_0, \dots, \lambda_{\ell-1})$ and $\boldsymbol{\mu} = (\mu_0, \dots, \mu_{\ell-1})$ are the scaled dual variables (by $1/\rho$) and $\rho > 0$ is the augmentation constant. Note that we have only relaxed the equality constraints in (6), and the constraints describing the sets \mathcal{S}_{ϕ_k} as well as \mathcal{X} are kept intact. Furthermore, the inclusion of augmentation will render the dual function differentiable (see the Appendix for more details), and hence, easier to optimize.

For the Lagrangian in (7), the dual function, which provides a lower bound to p_{relaxed}^* , is given by $d(\boldsymbol{\lambda}, \boldsymbol{\mu}) = \inf_{(\mathbf{x}, \mathbf{y}, \mathbf{z})} \mathcal{L}(\mathbf{x}, \mathbf{y}, \mathbf{z}, \boldsymbol{\lambda}, \boldsymbol{\mu})$. The best lower bound can then be found by maximizing the dual function. If strong duality holds, then this best lower bound would match p_{relaxed}^* .

Solving the inner problem jointly over $(\mathbf{x}, \mathbf{y}, \mathbf{z})$ to find the dual function is as difficult as solving a direct convex relaxation of (3). Instead, we split the primal variables $(\mathbf{x}, \mathbf{y}, \mathbf{z})$ into \mathbf{x} and (\mathbf{y}, \mathbf{z}) and apply the classical ADMM algorithm to obtain the following iterations (shown in Figure 1) for updating the primal and dual variables,

$$\mathbf{x}^+ \in \operatorname{argmin}_{\mathbf{x}} \mathcal{L}(\mathbf{x}, \mathbf{y}, \mathbf{z}, \boldsymbol{\lambda}, \boldsymbol{\mu}) \quad (8a)$$

$$(\mathbf{y}^+, \mathbf{z}^+) \in \operatorname{argmin}_{(\mathbf{y}, \mathbf{z})} \mathcal{L}(\mathbf{x}^+, \mathbf{y}, \mathbf{z}, \boldsymbol{\lambda}, \boldsymbol{\mu}) \quad (8b)$$

$$(\boldsymbol{\lambda}^+, \boldsymbol{\mu}^+) = (\boldsymbol{\lambda}, \boldsymbol{\mu}) + \nabla_{(\boldsymbol{\lambda}, \boldsymbol{\mu})} \mathcal{L}(\mathbf{x}^+, \mathbf{y}^+, \mathbf{z}^+, \boldsymbol{\lambda}, \boldsymbol{\mu}). \quad (8c)$$

As we show below, the Lagrangian has a separable structure by construction that can be exploited in order to efficiently implement each step of (8).

2.3 The x-update

The Lagrangian in (7) is separable across the x_k variables; hence, the minimization in (8a) can be done independently for each x_k . Specifically, for $k = 0$, we obtain the following update rule for x_0 ,

$$x_0^+ = \text{Proj}_{\mathcal{X}}(y_0 - \lambda_0). \quad (9a)$$

Projections onto the ℓ_∞ and ℓ_2 balls can be done in closed-form. For the ℓ_1 ball, we can use the efficient projection scheme proposed in [8], which has $\mathcal{O}(n_0)$ complexity in expectation.

For subsequent layers $k = 1, \dots, \ell$ we obtain the updates

$$x_k^+ = \frac{1}{2}(y_k - \lambda_k + z_{k-1} - \mu_{k-1}) \quad (9b)$$

$$x_\ell^+ = \arg \min_{x_\ell} J(x_\ell) + \frac{\rho}{2} \|x_\ell - z_{\ell-1} + \mu_{\ell-1}\|_2^2. \quad (9c)$$

For convex J and $\rho > 0$, the optimization problem for updating x_ℓ is strongly convex with a unique optimal solution. Indeed, its solution is the proximal operator of J/ρ evaluated at $z_{\ell-1} - \mu_{\ell-1}$. For the special case of linear objectives, $J(x_\ell) = c^\top x_\ell$, we obtain the closed-form solution $x_\ell^+ = -c/\rho + (z_{\ell-1} - \mu_{\ell-1})$.

2.4 The (y, z)-update

Similarly, the Lagrangian is also separable across the (y_k, z_k) variables. Updating these variables in (8b) corresponds to the following projection operations per layer,

$$(y_k^+, z_k^+) = \text{Proj}_{\mathcal{S}_{\phi_k}}(x_k^+ + \lambda_k, x_{k+1}^+ + \mu_k), \quad (10)$$

for $k = 0, \dots, \ell - 1$. Depending on the type of the layer (linear, activation, convolution, etc.), we obtain different projections, which we describe below.

Affine Layers. Suppose $\phi_k(y_k) = W_k y_k + b_k$ is an affine layer representing a fully-connected, convolutional, or an average pooling layer. Then the graph of ϕ_k is already a convex set given by $\mathcal{G}_{\phi_k} = \{(y_k, z_k) \mid z_k = W_k y_k + b_k\}$. Choosing $\mathcal{S}_{\phi_k} = \mathcal{G}_{\phi_k}$, the projection in (10) takes the form

$$\begin{aligned} y_k^+ &= (I_{n_k} + W_k^\top W_k)^{-1}(x_k^+ + \lambda_k + W_k^\top(x_{k+1}^+ + \mu_k - b_k)) \\ z_k^+ &= W_k y_k^+ + b_k. \end{aligned} \quad (11)$$

The matrix $(I_{n_k} + W_k^\top W_k)^{-1}$ can be pre-computed and cached for subsequent iterations. We can do this efficiently for convolutional layers using the fast Fourier transform, which we discuss later in Section C.3.

Activation Layers. For an activation layer of the form $\phi(x) := [\varphi_1(x_1) \cdots \varphi_n(x_n)]^\top$, the convex relaxation of \mathcal{G}_ϕ is given by the Cartesian product of individual convex relaxations i.e., $\mathcal{S}_\phi = \mathcal{S}_{\varphi_1} \times \cdots \times \mathcal{S}_{\varphi_n}$. For a generic activation function $\varphi: \mathbb{R} \rightarrow \mathbb{R}$, suppose we have a concave upper bound $\bar{\varphi}$ and a convex lower bound $\underline{\varphi}$ on φ over an interval $I = [\underline{x}, \bar{x}]$, i.e., $\underline{\varphi}(x) \leq \varphi(x) \leq \bar{\varphi}(x) \forall x \in [\underline{x}, \bar{x}]$. A convex overapproximation of \mathcal{G}_φ is

$$\mathcal{S}_\varphi = \{(x, y) \mid \underline{\varphi}(x) \leq y \leq \bar{\varphi}(x), \underline{x} \leq x \leq \bar{x}\}, \quad (12)$$

which turns out to be the convex hull of $\mathcal{G}(\varphi)$ when $\bar{\varphi}$ and $\underline{\varphi}$ are concave and convex envelopes of φ , respectively. As an example, when $\underline{x} < 0 < \bar{x}$, the ReLU activation function $y = \max(0, x)$ admits the envelopes $\underline{\varphi}(x) = \max(0, x)$, $\bar{\varphi}(x) = \underline{y} + \frac{\bar{y} - \underline{y}}{\bar{x} - \underline{x}}(x - \underline{x})$ on $[\underline{x}, \bar{x}]$, where $\underline{y} = \max(0, \underline{x})$ and $\bar{y} = \max(0, \bar{x})$ [11, 36] (see Figure 1). The assumed pre-activation bounds \underline{x} and \bar{x} used to relax the activation functions can be obtained a priori via a variety of existing techniques [36, 41, 43]. We present projection operators of additional layers in Appendix B.

2.5 The (λ, μ) -update

Finally, we update the scaled dual variables as follows,

$$\begin{aligned}\lambda_k^+ &= \lambda_k + (x_k^+ - y_k^+) & k = 0, \dots, \ell - 1 \\ \mu_k^+ &= \mu_k + (x_{k+1}^+ - z_k^+) & k = 0, \dots, \ell - 1.\end{aligned}\tag{13}$$

The DeepSplit Algorithm is summarized in Algorithm 1. We provide further details such as stopping criteria, parameter selection, and efficient implementations for convolutional layers in Appendix C.

3 Connection to Lagrangian-based Methods

In this section, we draw connections to two related methods relying on Lagrangian relaxation. Specifically, we relate our approach to an earlier dual method [10] (Section 3.1), as well as a recent Lagrangian decomposition method [2] (Section 3.2). Overall, these approaches use a similar Lagrangian formulation, but the specific choices in splitting and augmentation of the Lagrangian result in poorer theoretical convergence guarantees when solving the convex relaxation to optimality.

3.1 Lagrangian Relaxation and Dual Subgradient Method

Instead of splitting the neural network equations in (3) with auxiliary variables, an alternative strategy is to directly relax the equations with Lagrangian multipliers [10]:

$$\mathcal{L}(\mathbf{x}, \boldsymbol{\lambda}) = J(x_\ell) + \sum_{k=0}^{\ell-1} \lambda_k^\top (x_{k+1} - \phi_k(x_k)) + \mathbb{I}_{\mathcal{X}}(x_0).\tag{14}$$

where $\mathbf{x} = (x_0, \dots, x_\ell)$ and $\boldsymbol{\lambda} = (\lambda_0, \dots, \lambda_{\ell-1})$. This results in the dual problem $d_{\mathcal{O}}^* \leftarrow \text{maximize } g(\boldsymbol{\lambda})$, where the dual function is

$$g(\boldsymbol{\lambda}) = \inf_{x_\ell \leq x_\ell \leq \bar{x}_\ell} \{J(x_\ell) + \lambda_{\ell-1}^\top x_\ell\} + \sum_{k=1}^{\ell-1} \inf_{x_k \leq x_k \leq \bar{x}_k} \{\lambda_{k-1}^\top x_k - \lambda_k^\top \phi_k(x_k)\} + \inf_{x_0 \in \mathcal{X}_0} \{-\lambda_0^\top \phi_0(x_0)\}.$$

By weak duality, $d_{\mathcal{O}}^* \leq p^*$. The inner minimization problems in $g(\boldsymbol{\lambda})$ to compute the dual function for a given $\boldsymbol{\lambda}$ can often be solved efficiently or even in closed-form [10]. The resulting dual problem is unconstrained but non-differentiable; hence it is solved using dual subgradient method [10]. However, subgradient methods are known to be very slow; their convergence rate is $O(1/\sqrt{N})$ where N is the number of updates [24], making it an inefficient solver for finding exact solutions to the convex relaxation. On the other hand, this method can be stopped at any time to obtain a valid lower bound.

3.2 Augmented Lagrangian and Method of Multipliers

Another related approach is the Lagrangian decomposition method from [2]. To decouple the constraints for the convex relaxation of (3), this approach can be viewed as introducing *one* set of intermediate variables y_k as copies of x_k to obtain

$$\begin{aligned}p_{relaxed}^* &\leftarrow \text{minimize} && J(y_\ell) \\ &\text{subject to} && (y_k, x_{k+1}) \in \mathcal{S}_{\phi_k} && k = 0, \dots, \ell - 1 \\ &&& y_k = x_k && k = 0, \dots, \ell \\ &&& x_0 \in \mathcal{X}\end{aligned}\tag{15}$$

This splitting is in the spirit of the splitting introduced in [2,3],¹ and differs from our splitting which uses *two* sets of variables in (5). By relaxing the consensus constraints $y_k = x_k$, the Lagrangian is

$$\mathcal{L}(\mathbf{x}, \mathbf{y}, \boldsymbol{\mu}) = J(y_\ell) + \sum_{k=0}^{\ell} \mu_k^\top (y_k - x_k) + \sum_{k=0}^{\ell-1} \mathbb{I}_{\mathcal{S}_{\phi_k}}(y_k, x_{k+1}) + \mathbb{I}_{\mathcal{X}}(x_0). \quad (16)$$

Again the Lagrangian is separable and its minimization results in the following dual function

$$g(\boldsymbol{\mu}) = \inf_{\underline{x}_\ell \leq y_\ell \leq \bar{x}_\ell} \{J(y_\ell) + \mu_\ell^\top y_\ell\} + \sum_{k=0}^{\ell-1} \inf_{(y_k, x_{k+1}) \in \mathcal{S}_{\phi_k}} \{\mu_k^\top y_k - \mu_{k+1}^\top x_{k+1}\} + \inf_{x_0 \in \mathcal{X}} \{-\mu_0^\top x_0\}.$$

Since the dual function is not differentiable, it must be maximized by a subgradient method, which again has an $O(1/\sqrt{N})$ rate. To induce differentiability in the dual function and improve speed, [2] uses Augmented Lagrangian (AL). Since only one set of variables was introduced in (15), the AL is no longer separable across the primal variables. Therefore, for each update of the dual variable, the AL must be minimized iteratively. To this end, the authors in [2] use the Frank Wolfe Algorithm in a block-coordinate as an iterative subroutine. However, this slows down overall convergence and suffers from compounding errors when the sub-problems are not fully solved.

In contrast to this approach, in this paper we used a different variable splitting scheme in (5) that allows us to *fully* separate layers in a neural network. This subtle difference has a significant impact: we can efficiently minimize the corresponding AL in *closed form*, without resorting to any iterative subroutine. Specifically, we use the ADMM algorithm, which is known to converge at an $O(1/N)$ rate [18]. In summary, our method enjoys an order of magnitude faster theoretical convergence, is more robust to numerical errors, and has minimal requirements for parameter tuning. However, ADMM does not enjoy the anytime property of the previous two methods described above.

4 Experiments

The strengths of our method, DeepSplit, are (a) its ability to exactly solve LP relaxations and (b) do so at scales that were previously impossible. To evaluate this, we first demonstrate how solving the LP to optimality leads to tighter certified robustness guarantees in image classification and reinforcement learning tasks (Section 4.1). We then stress test our method in both speed and scalability against a commercial LP solver and in the large network setting (Section 4.2).

Setup In all the experiments, we focus on the setting of *verification-agnostic* networks, similar to [6]. However, we focus on significantly *larger* networks that have previously only been feasibly bounded with fast linear-based bounds of the LP relaxation [38, 39]. All the networks have been trained adversarially with the PGD attack [23]. Full details about the network architecture, network training, and the parameters for our splitting method can be found in Appendix E.

4.1 Improved Bounds From Exact LP Solutions

We first demonstrate how solving the LP exactly with our method results in tighter bounds than prior work. We consider two main settings: certifying the robustness of classifiers for CIFAR10 and deep Q-networks (DQNs) in Atari games. We defer additional analogous results in the smaller MNIST setting to Appendix E.3.

¹If we define $\phi_k(x_k) = W_{k+1}\sigma(x_k) + b_{k+1}$, where W_{k+1}, b_{k+1} are the parameters of the affine layer and σ is a layer of activation functions, this splitting coincides with the one proposed in [2, 3]

CIFAR10 Much work studying verification of deep networks in the CIFAR10 setting [7, 31, 33], including the more scalable Lagrangian-based methods [2, 10], have focused primarily on a CNN with only 6k hidden units from [36]—smaller than the LeNet architecture used for MNIST [21]. Consequently, the LP relaxation for this network can be solved exactly with a commercial LP solver such as Gurobi, and recent SDP solvers can produce even tighter bounds [6], rendering any LP-based solutions for this network obsolete.

Instead, we consider a much larger architecture from [38] (an order of magnitude larger), which cannot be feasibly solved by Gurobi nor the SDP solver [6]. Up until this point, the only solutions in the literature that have verified networks of this size are linear-based bounds to the LP relaxation [38, 39]. However, these bounds are known to be quite loose. How much better can we do if we solve the LP exactly?

In Table 1, we report the certified accuracy of solving the LP exactly with ADMM in comparison to a range of baselines. Specifically, we show results using the exact LP solution (ADMM) from our solver, and compare with methods that have previously demonstrated the ability to bound networks of this size: fast bounds of the LP (Linear) [38, 39], and interval bounds (IBP) [17]. We additionally compare to a suite of Lagrangian-based methods [2, 10], whose effectiveness at this scale was previously unknown. These Lagrangian methods include supergradient ascent with the Adam [3] (Adam), dual supergradient ascent [10] (Dual Adam) and a variant thereof (Dual Decomposition Adam) [3], and a proximal method (Prox) [2].

We find that solving the LP exactly can in fact lead to substantial gains in certified robustness for large networks, with up to 5% additional certified robustness over the best-performing alternative. We further note that, unlike previous work [28] that spent multiple CPU-years of compute to study exact solutions to the LP in the *small* network setting, our ADMM solver is able to verify an order of magnitude *larger* network over the entire test set and multiple epsilons in 25 hours on a single GPU.

Table 1: Certified test accuracy (%) of PGD-trained models on CIFAR10 through ADMM, the Lagrangian decomposition methods [3, 10], and fast dual/linear [38, 39] or interval bounds [17].

ϵ	Exact	Lagrangian methods				Fast bounds	
	ADMM	Adam [2]	Prox [2]	Dual Adam [10]	Dual Decomposition Adam [2]	Linear [38, 39]	IBP [17]
1/255	64.0	44.7	59.7	45.2	45.7	59.8	42.8
1.5/255	45.7	26.1	39.5	26.6	27.0	36.8	16.8
2/255	19.5	9.7	15.9	9.9	10.1	13.2	3.62
2.5/255	5.5	2.2	4.0	2.3	2.4	3.3	0.7

State-robust RL We demonstrate our approach on a non-classification benchmark from reinforcement learning: verifying the robustness of deep Q-networks (DQNs) to adversarial state perturbations [42]. Specifically, we verify whether a learned DQN policy outputs stable actions in the discrete space when given perturbed states. Similar to the large network considered in the CIFAR10 setting, the networks we consider have only been demonstrably verified with fast, linear-based bounds [39] and are simply too large to be solved with the SDP solver or an LP solver like Gurobi.

We consider three Atari game benchmarks: BankHeist, Roadrunner, and Pong ² and verify pretrained DQNs which were trained with PGD-adversarial training [42]. For each benchmark, we

² [42] consider one additional RL setting (Freeway). However, the released PGD-trained DQN is completely unverifiable for nearly all epsilons that we considered.

Table 2: The percentage of actions from a deep Q-network that are certifiably robust to changes in the state space for various RL tasks.

Bankheist			Roadrunner			Pong		
ϵ	Linear [38,39]	ADMM	ϵ	Linear [38,39]	ADMM	ϵ	Linear [38,39]	ADMM
0.0016	67.0	71.4	0.0012	32.6	36.6	0.0004	96.1	97.4
0.0020	39.7	49.5	0.0016	26.3	27.5	0.0008	93.4	95.6
0.0024	12.7	25.9	0.0020	19.6	22.8	0.0012	92.1	94.3
0.0027	1.4	7.3	0.0024	1.1	3.7	0.0016	82.1	84.0

verify the robustness of the DQN over 10,000 randomly sampled frames as our test dataset. Further details regarding the dataset, the DQN architectures, and this task can be found in Appendix E.4.

Similar to the CIFAR10 setting, we observe consistent improvement in certified robustness of the DQN when solving the LP exactly with ADMM. We summarize the results using our method and the linear-based bounds on LP relaxations [38,39] in Table 2.

4.2 Speed and Scalability

In this section, we stress test several aspects of DeepSplit for solving LP relaxations. We first measure how it compares to other exact solvers for convex relaxations, namely a commercial LP solver and a specialized SDP solver, in small settings that these solvers can handle. We then push the limits of architecture size and measure the improvement in bounds for a standard ResNet18.

Speed comparison We first compare the solving speeds of our method with exact solvers for convex relaxations of deep networks: a commercial-grade LP solver, Gurobi, and specialized SDP-solvers [6]. We benchmark these exact solvers on two tasks: calculating intermediate bounds on a fully connected network that Gurobi can handle, and verifying a small convolutional architecture that the SDP-solver can handle (see Appendix G for further details on experimental setup).

We first find that our method provides a nearly 7x speedup over commercial-grade LP solvers. On average, it takes ADMM 38 seconds per example to calculate these intermediate bounds using a single GeForce GTX 1080, in comparison to 258 seconds per example for Gurobi on an Intel Core i7-6700K. We additionally find that our LP solver is 30x faster than the SDP solver [6]. Specifically, we can solve LP relaxations at 0.2 hours per thousand examples, whereas the SDP relaxation takes 6 hours per thousand examples. This highlights the trade-off in speed and scalability of solving different relaxations: SDPs can produce tighter bounds but LPs are substantially faster to solve.

Scalability Finally, to test the scalability and generality of our approach, we consider solving the LP relaxation for a ResNet18, which up to this point has simply not been possible. The only applicable method here is LiRPA [39]—a highly scalable implementation of the linear-based bounds that works for arbitrary networks. For this experiment, we measure how much tighter of a bound we can get from solving the LP exactly in comparison to LiRPA (see Appendix H for details). We find that solving the LP relaxation exactly with our ADMM solver can produce substantial improvements in the bound even at ResNet18 scales. For each possible bound in the network, we calculate the exact LP relaxation with ADMM and the corresponding LiRPA bound, and plot each pair in Figure 2. We find that ADMM can find significantly tighter bounds for a substantial number of examples.

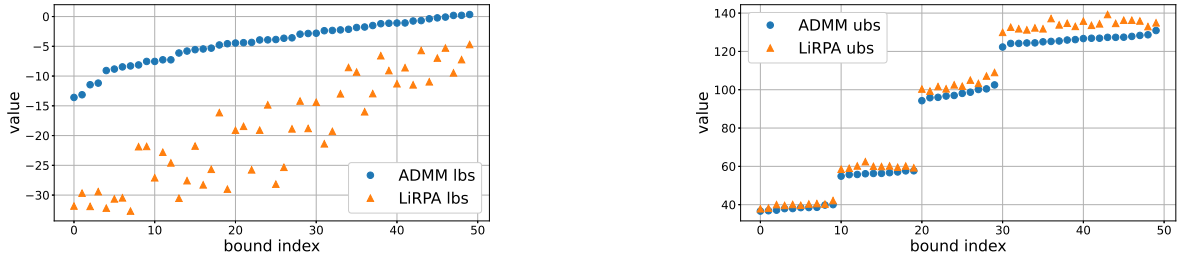


Figure 2: ResNet18 output lower (left) and upper (right) bounds obtained using either ADMM (blue dots) and LiRPA (orange triangles). Higher lower bounds and lower upper bounds are better. For ease of visualization, bounds are sorted in ascending order according to the ADMM bound.

5 Conclusion

In this paper, we proposed DeepSplit, a scalable and modular operator splitting technique for solving convex relaxation-based verification problems for neural networks. By splitting the problem into separable sub-problems with analytical or easy-to-compute solutions, the method can solve large-scale LP relaxations with GPU acceleration with favorable convergence rates. Using this methodology, we can solve LP relaxations exactly and obtain significantly tighter bounds in verification problems for large networks that were previously impossible to solve exactly due to their size. Even on relatively small problem instances, our approach can solve LP relaxations almost 7x faster than state-of-the-art commercial solvers with just a single GPU. This speedup can directly accelerate complete verifiers for deep learning by providing tighter and faster solutions to commonly used LP subroutines (e.g. those used in branch-and-bound solvers for MILPs), without needing to rely on excessive computational power. Finally, many variations of ADMM have been proposed to improve convergence rates, such as over-relaxation [1], adaptive penalty parameter [40], and acceleration techniques [16, 44]. We leave as future work a further investigation of whether these techniques can also help improve convergence rates in deep learning-sized problem instances, as well as extensions beyond the LP setting.

Broader impact & limitations A limitation of this work is that the tightness of the bounds are not as tight as e.g. SDP solvers or other approaches. This is a necessary trade-off that we make in order to scale to large networks whose LP relaxation was previously impossible to solve, let alone other tighter relaxations. It is possible that users may use our work to argue that their models are robust and thus trustworthy. We emphasize that one should not over-generalize from the robustness guarantees that we enable. Our method, like many others, verify well-defined properties that do not necessarily imply general robustness.

References

- [1] Stephen Boyd, Neal Parikh, and Eric Chu. *Distributed optimization and statistical learning via the alternating direction method of multipliers*. Now Publishers Inc, 2011.
- [2] Rudy Bunel, Alessandro De Palma, Alban Desmaison, Krishnamurthy Dvijotham, Pushmeet Kohli, Philip Torr, and M Pawan Kumar. Lagrangian decomposition for neural network verification. In *Conference on Uncertainty in Artificial Intelligence*, pages 370–379. PMLR, 2020.

- [3] Rudy Bunel, Jingyue Lu, Ilker Turkaslan, Pushmeet Kohli, P Torr, and P Mudigonda. Branch and bound for piecewise linear neural network verification. *Journal of Machine Learning Research*, 21(2020), 2020.
- [4] Yulong Cao, Chaowei Xiao, Benjamin Cyr, Yimeng Zhou, Won Park, Sara Rampazzi, Qi Alfred Chen, Kevin Fu, and Z Morley Mao. Adversarial sensor attack on lidar-based perception in autonomous driving. In *Proceedings of the 2019 ACM SIGSAC conference on computer and communications security*, pages 2267–2281, 2019.
- [5] Chih-Hong Cheng, Georg Nührenberg, and Harald Ruess. Maximum resilience of artificial neural networks. In *International Symposium on Automated Technology for Verification and Analysis*, pages 251–268. Springer, 2017.
- [6] Sumanth Dathathri, Krishnamurthy Dvijotham, Alexey Kurakin, Aditi Raghunathan, Jonathan Uesato, Rudy Bunel, Shreya Shankar, Jacob Steinhardt, Ian Goodfellow, Percy Liang, et al. Enabling certification of verification-agnostic networks via memory-efficient semidefinite programming. *arXiv preprint arXiv:2010.11645*, 2020.
- [7] Alessandro De Palma, Harkirat Singh Behl, Rudy Bunel, Philip HS Torr, and M Pawan Kumar. Scaling the convex barrier with active sets. *arXiv preprint arXiv:2101.05844*, 2021.
- [8] John Duchi, Shai Shalev-Shwartz, Yoram Singer, and Tushar Chandra. Efficient projections onto the l_1 -ball for learning in high dimensions. In *Proceedings of the 25th international conference on Machine learning*, pages 272–279, 2008.
- [9] Souradeep Dutta, Susmit Jha, Sriram Sankaranarayanan, and Ashish Tiwari. Output range analysis for deep feedforward neural networks. In *NASA Formal Methods Symposium*, pages 121–138. Springer, 2018.
- [10] Krishnamurthy Dvijotham, Robert Stanforth, Sven Gowal, Timothy Mann, and Pushmeet Kohli. A dual approach to scalable verification of deep networks. *arXiv preprint arXiv:1803.06567*, 2018.
- [11] Ruediger Ehlers. Formal verification of piece-wise linear feed-forward neural networks. In *International Symposium on Automated Technology for Verification and Analysis*, pages 269–286. Springer, 2017.
- [12] Mahyar Fazlyab, Manfred Morari, and George J Pappas. Safety verification and robustness analysis of neural networks via quadratic constraints and semidefinite programming. *IEEE Transactions on Automatic Control*, 2020.
- [13] Mahyar Fazlyab, Alexander Robey, Hamed Hassani, Manfred Morari, and George J Pappas. Efficient and accurate estimation of lipschitz constants for deep neural networks. *arXiv preprint arXiv:1906.04893*, 2019.
- [14] Samuel G Finlayson, John D Bowers, Joichi Ito, Jonathan L Zittrain, Andrew L Beam, and Isaac S Kohane. Adversarial attacks on medical machine learning. *Science*, 363(6433):1287–1289, 2019.
- [15] Matteo Fischetti and Jason Jo. Deep neural networks and mixed integer linear optimization. *Constraints*, 23(3):296–309, 2018.

- [16] Anqi Fu, Junzi Zhang, and Stephen Boyd. Anderson accelerated douglas–rachford splitting. *SIAM Journal on Scientific Computing*, 42(6):A3560–A3583, 2020.
- [17] Sven Gowal, Krishnamurthy Dvijotham, Robert Stanforth, Rudy Bunel, Chongli Qin, Jonathan Uesato, Timothy Mann, and Pushmeet Kohli. On the effectiveness of interval bound propagation for training verifiably robust models. *arXiv preprint arXiv:1810.12715*, 2018.
- [18] Bingsheng He and Xiaoming Yuan. On the $o(1/n)$ convergence rate of the douglas–rachford alternating direction method. *SIAM Journal on Numerical Analysis*, 50(2):700–709, 2012.
- [19] BS He, Hai Yang, and SL Wang. Alternating direction method with self-adaptive penalty parameters for monotone variational inequalities. *Journal of Optimization Theory and applications*, 106(2):337–356, 2000.
- [20] Guy Katz, Clark Barrett, David L Dill, Kyle Julian, and Mykel J Kochenderfer. Reluplex: An efficient smt solver for verifying deep neural networks. In *International Conference on Computer Aided Verification*, pages 97–117. Springer, 2017.
- [21] Yann LeCun et al. Lenet-5, convolutional neural networks. URL: <http://yann.lecun.com/exdb/lenet>, 20(5):14, 2015.
- [22] Alessio Lomuscio and Lalit Maganti. An approach to reachability analysis for feed-forward relu neural networks. *arXiv preprint arXiv:1706.07351*, 2017.
- [23] Aleksander Madry, Aleksandar Makelov, Ludwig Schmidt, Dimitris Tsipras, and Adrian Vladu. Towards deep learning models resistant to adversarial attacks. *arXiv preprint arXiv:1706.06083*, 2017.
- [24] Yurii Nesterov. *Introductory lectures on convex optimization: A basic course*, volume 87. Springer Science & Business Media, 2003.
- [25] Brendan O’donoghue, Eric Chu, Neal Parikh, and Stephen Boyd. Conic optimization via operator splitting and homogeneous self-dual embedding. *Journal of Optimization Theory and Applications*, 169(3):1042–1068, 2016.
- [26] Brendan O’Donoghue, Giorgos Stathopoulos, and Stephen Boyd. A splitting method for optimal control. *IEEE Transactions on Control Systems Technology*, 21(6):2432–2442, 2013.
- [27] Aditi Raghunathan, Jacob Steinhardt, and Percy S Liang. Semidefinite relaxations for certifying robustness to adversarial examples. In *Advances in Neural Information Processing Systems*, pages 10900–10910, 2018.
- [28] Hadi Salman, Greg Yang, Huan Zhang, Cho-Jui Hsieh, and Pengchuan Zhang. A convex relaxation barrier to tight robustness verification of neural networks. *arXiv preprint arXiv:1902.08722*, 2019.
- [29] Karsten Scheibler, Leonore Winterer, Ralf Wimmer, and Bernd Becker. Towards verification of artificial neural networks. In *MBMV*, pages 30–40, 2015.
- [30] Michel Schubiger, Goran Banjac, and John Lygeros. Gpu acceleration of admm for large-scale quadratic programming. *Journal of Parallel and Distributed Computing*, 144:55–67, 2020.

- [31] Gagandeep Singh, Rupanshu Ganvir, Markus Püschel, and Martin Vechev. Beyond the single neuron convex barrier for neural network certification. *Advances in Neural Information Processing Systems*, 32:15098–15109, 2019.
- [32] Gavin Taylor, Ryan Burmeister, Zheng Xu, Bharat Singh, Ankit Patel, and Tom Goldstein. Training neural networks without gradients: A scalable admm approach. In *International conference on machine learning*, pages 2722–2731. PMLR, 2016.
- [33] Christian Tjandraatmadja, Ross Anderson, Joey Huchette, Will Ma, Krupal Patel, and Juan Pablo Vielma. The convex relaxation barrier, revisited: Tightened single-neuron relaxations for neural network verification. *arXiv preprint arXiv:2006.14076*, 2020.
- [34] Vincent Tjeng, Kai Xiao, and Russ Tedrake. Evaluating robustness of neural networks with mixed integer programming. *arXiv preprint arXiv:1711.07356*, 2017.
- [35] Tsui-Wei Weng, Huan Zhang, Hongge Chen, Zhao Song, Cho-Jui Hsieh, Duane Boning, Inderjit S Dhillon, and Luca Daniel. Towards fast computation of certified robustness for relu networks. *arXiv preprint arXiv:1804.09699*, 2018.
- [36] Eric Wong and J Zico Kolter. Provable defenses against adversarial examples via the convex outer adversarial polytope. *arXiv preprint arXiv:1711.00851*, 1(2):3, 2017.
- [37] Eric Wong, Leslie Rice, and J Zico Kolter. Fast is better than free: Revisiting adversarial training. *arXiv preprint arXiv:2001.03994*, 2020.
- [38] Eric Wong, Frank R Schmidt, Jan Hendrik Metzen, and J Zico Kolter. Scaling provable adversarial defenses. *arXiv preprint arXiv:1805.12514*, 2018.
- [39] Kaidi Xu, Zhouxing Shi, Huan Zhang, Yihan Wang, Kai-Wei Chang, Minlie Huang, Bhavya Kailkhura, Xue Lin, and Cho-Jui Hsieh. Automatic perturbation analysis for scalable certified robustness and beyond. *Advances in Neural Information Processing Systems*, 33, 2020.
- [40] Zheng Xu, Mario Figueiredo, and Tom Goldstein. Adaptive admm with spectral penalty parameter selection. In *Artificial Intelligence and Statistics*, pages 718–727. PMLR, 2017.
- [41] Huan Zhang, Hongge Chen, Chaowei Xiao, Sven Gowal, Robert Stanforth, Bo Li, Duane Boning, and Cho-Jui Hsieh. Towards stable and efficient training of verifiably robust neural networks. *arXiv preprint arXiv:1906.06316*, 2019.
- [42] Huan Zhang, Hongge Chen, Chaowei Xiao, Bo Li, Duane Boning, and Cho-Jui Hsieh. Robust deep reinforcement learning against adversarial perturbations on observations. *Advances in Neural Information Processing Systems*, 2020.
- [43] Huan Zhang, Tsui-Wei Weng, Pin-Yu Chen, Cho-Jui Hsieh, and Luca Daniel. Efficient neural network robustness certification with general activation functions. *arXiv preprint arXiv:1811.00866*, 2018.
- [44] Juyong Zhang, Yue Peng, Wenqing Ouyang, and Bailin Deng. Accelerating admm for efficient simulation and optimization. *ACM Transactions on Graphics (TOG)*, 38(6):1–21, 2019.
- [45] Yang Zheng, Giovanni Fantuzzi, Antonis Papachristodoulou, Paul Goulart, and Andrew Wynn. Fast admm for semidefinite programs with chordal sparsity. In *2017 American Control Conference (ACC)*, pages 3335–3340. IEEE, 2017.

A ADMM for General Computational Graphs

To handle general computational graphs, we follow the approach used in [38]. Specifically, consider a generalized ℓ -"layer" neural network given by the equations

$$x_{k+1} = \sum_{i=1}^k \phi_{ik}(x_i) \equiv \Phi_k(x_{1:k}) \quad k = 0, \dots, \ell - 1 \quad (17)$$

where $x_{1:k}$ denotes the concatenated vector of variables (x_1, \dots, x_k) . Note that this view of a network reduces to the feedforward equations in (2) when $\phi_{ik}(x_i) = 0$ for all $i < k$. Furthermore, this view subsumes arbitrary skip connections, such as residual connections. Then, the graph form of the verification problem in (4) can be rewritten for the generalized neural network as

$$\begin{aligned} p^* \leftarrow \text{minimize} \quad & J(x_\ell) \\ \text{subject to} \quad & (x_{1:k}, x_{k+1}) \in \mathcal{G}_{\phi_k(x_{1:k})} \quad k = 0, \dots, \ell - 1 \\ & x_0 \in \mathcal{X}. \end{aligned} \quad (18)$$

Similar to before, let \mathcal{S}_{ϕ_k} be a sound convex approximation of \mathcal{G}_{ϕ_k} . Then, our convex relaxation introduces additional intermediate variables $y_{1:k}$ and z_k to get the following convex relaxation (analogous to (6)):

$$\begin{aligned} p_{\text{relaxed}}^* \leftarrow \text{minimize} \quad & J(x_\ell) \\ \text{subject to} \quad & y_{1:k} = x_{1:k} \quad k = 0, \dots, \ell - 1 \\ & (y_{1:k}, z_k) \in \mathcal{S}_{\phi_k} \quad k = 0, \dots, \ell - 1 \\ & x_{k+1} = z_k \quad k = 0, \dots, \ell - 1 \\ & x_0 \in \mathcal{X}. \end{aligned} \quad (19)$$

Thus, producing an ADMM layer for a network with arbitrary skip connections reduces to deriving the corresponding projection operator onto \mathcal{S}_{ϕ_k} . Since most residual connections simply add an affine transformation of a previous layer, these projections are straightforward and have a closed form (an example of a typical residual ADMM block is in Appendix B).

B ADMM layers

B.1 ReLU projection

Consider the ReLU function $y = \varphi(x) = \max(0, x)$ on the interval $x \in [\underline{x}, \bar{x}]$. The projection of a point $(x^{(0)}, y^{(0)})$ onto the convex hull of $G(\varphi)$ has a closed-form solution. We consider three cases.

1. Active neuron ($\underline{x} \geq 0$). In this case, the convex hull is given by

$$\mathcal{S}_\varphi = \{(x, y) \mid y = x, \underline{x} \leq x \leq \bar{x}\}.$$

and the projection of $(x^{(0)}, y^{(0)})$ onto \mathcal{S}_φ is given by $x' = y' = \min(\max(\frac{x^{(0)} + y^{(0)}}{2}, \underline{x}), \bar{x})$.

2. Inactive neuron ($\bar{x} \leq 0$). In this case, the convex hull is

$$\mathcal{S}_\varphi = \{(x, y) \mid y = 0, \underline{x} \leq x \leq \bar{x}\}.$$

and the projection of $(x^{(0)}, y^{(0)})$ onto \mathcal{S}_φ is given by $x' = \min(\max(x^{(0)}, \underline{x}), \bar{x})$, $y' = 0$.

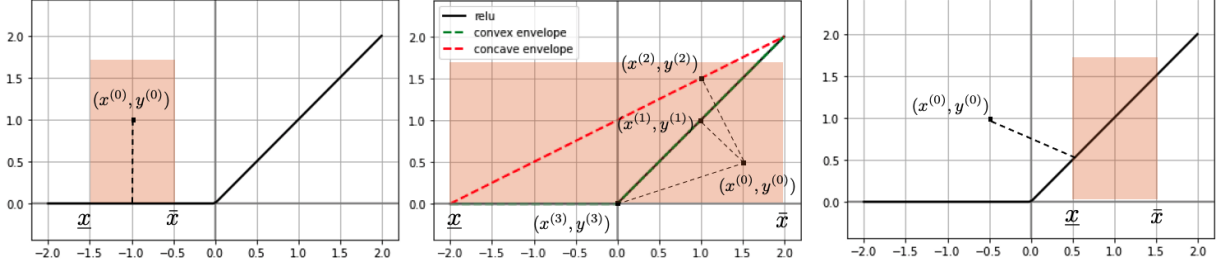


Figure 3: Projection of a point (x_0, y_0) onto the convex hull of the ReLU function $y = \max(0, x)$ over the interval $[\underline{x}, \bar{x}]$. We first project (x_0, y_0) onto all facets of the convex hull and then select the point with minimal distance to (x_0, y_0) .

3. Unknown neuron ($\underline{x} \leq 0 \leq \bar{x}$). The convex hull is given by

$$\mathcal{S}_\varphi = \{(x, y) \mid y \geq 0, y \geq x, y \leq \underline{y} + s(x - \underline{x})\}$$

where $s = \frac{\bar{y} - \underline{y}}{\bar{x} - \underline{x}}$, $\underline{y} = \max(0, \underline{x})$, $\bar{y} = \max(0, \bar{x})$. We first project $(x^{(0)}, y^{(0)})$ onto each facet of the triangle and then select the point with the minimal distance.

$$\begin{aligned} x^{(1)} &= \min(\max(\frac{x^{(0)} + y^{(0)}}{2}, 0), \bar{x}) & y^{(1)} &= x^{(1)} \\ x^{(2)} &= \min(\max(\frac{x^{(0)} + sy^{(0)} + s(s\underline{x} - \underline{y})}{s^2 + 1}, \underline{x}), \bar{x}) & y^{(2)} &= \frac{s(x^{(0)} - \underline{x}) + s^2 y^{(0)} + \underline{y}}{s^2 + 1} \\ x^{(3)} &= \min(\max(0, x^{(0)}), \underline{x}) & y^{(3)} &= 0 \end{aligned}$$

The projected point is $(x', y') = (x^{(i^*)}, y^{(i^*)})$, where $i^* = \arg \min_{1 \leq i \leq 3} \sqrt{(x^{(0)} - x^{(i)})^2 + (y^{(0)} - y^{(i)})^2}$.

B.2 Convolutions

Although a convolution is technically a linear operator, it is impractical to directly form the inverse matrix from the projection step of the DeepSplit algorithm. Instead, we represent a typical convolutional layer f_{conv} with stride, padding and bias as

$$f_{\text{conv}} = f_{\text{bias}} \circ f_{\text{ds}} \circ f_{\text{crop}} \circ f_{\text{circ}} \circ f_{\text{pad}} = f_{\text{post}} \circ f_{\text{circ}} \circ f_{\text{pad}}, \quad (20)$$

where f_{pad} is a padding step, f_{circ} is a circular convolution step, f_{crop} is a cropping step, f_{ds} is a downsampling step to handle stride greater than one, and f_{bias} is a step that adds the bias. Then, the last three steps are combined into one post-processing step f_{post} to reduce the number of consensus constraints in the DeepSplit algorithm. The projection steps for all of these operators are presented next in Sections B.3 through B.6, and an efficient implementation of the projection step for the affine layer f_{circ} is in Appendix D.

B.3 Padding

The padding layer f_{pad} takes an image as input and adds padding to it. Denote the input image by y_k and the padded image by z_k . We can decompose the output z_k into two vectors, z_k^0 which is a

copy of the input y_k , and z_k^1 which represents the padded zeros on the edges of image. Equivalently, the padding layer $z_k = \phi_k(y_k)$ can be written in an affine form

$$z_k = \begin{bmatrix} z_k^0 \\ z_k^1 \end{bmatrix} = \begin{bmatrix} I \\ 0 \end{bmatrix} y_k = W_k y_k,$$

for which the projection operator reduces to the affine case.

B.4 Cropping

The cropping layer f_{crop} crops the output of the circular convolution f_{circ} to the original size of the input image before padding. Denote y_k the input image and z_k the output image of the cropping layer. By decomposing the input image y_k into the uncropped pixels y_k^0 and the cropped pixels y_k^1 , the cropping layer $z_k = \phi_k(y_k)$ has an affine formulation

$$z_k = y_k^0 = \begin{bmatrix} I & 0 \end{bmatrix} \begin{bmatrix} y_k^0 \\ y_k^1 \end{bmatrix} = W_k y_k$$

whose projection operator is given in Section 2.4.

B.5 Down-sampling and bias

If the typical convolutional layer f_{conv} has stride greater than one, a down-sampling layer is added in the DeepSplit algorithm, which essentially has the same affine form as the cropping layer with different values of y_k^0 and y_k^1 . Therefore, the projection operator for the down-sampling layer reduces to the affine case as well.

The bias layer in the DeepSplit algorithm handles the case when the convolutional layer f_{conv} has a bias b_k and is implemented by $z_k = \phi_k(y_k) = y_k + b_k$. This is an affine expression and its projection operator is given in Section 2.4.

B.6 Convolutional post-processing layer

We combine the cropping, down-sampling and bias layers into one post-processing layer, i.e., $f_{\text{post}} = f_{\text{bias}} \circ f_{\text{ds}} \circ f_{\text{crop}}$, as shown in (20). This reduces the total number of consensus constraints in the DeepSplit algorithm. Since all the three layers are in fact affine, the post-processing layer is also affine and its projection operator can be obtained correspondingly.

B.7 Maxpooling

Consider a Maxpooling layer $\phi(x) = \max_k x_k$, $k = 1, \dots, n$ over $\underline{x} \leq x \leq \bar{x}$. [3, Appendix B.2] shows that the Maxpooling layer can be equivalently decomposed as a combination of linear and ReLU layers. This is motivated by the following fact that $\max(x_1, x_2, x_3, x_4) = \max(\max(x_1, x_2), \max(x_3, x_4))$ and $\max(x_1, x_2) = \max(x_1 - x_2, 0) + \max(x_2 - x_1, 0) + \underline{x}_2$. Therefore, we can represent the Maxpooling layer by a composition of pairwise maximum functions which can themselves be decomposed into a combination of linear and ReLU layers. The projection operations onto the convex hull of the ReLU and linear layers are closed-form as shown in Appendix B.1 and Section 2.4, respectively.

B.8 Residual Connection

We consider a typical residual connection $\phi_k(y_k, y_i) = y_k + W_i y_i + b_i$ for $i < k$, where y_i is an arbitrary layer before y_k and W_i, b_i is any affine transformation (i.e. a 1 by 1 convolution for upsampling or downsampling layer frequently used in residual connections with differently sized feature maps). Then, we can write this as

$$\phi_k(y_{ki}) = W_{ki} y_{ki} + b_i, \quad (21)$$

where $y_{ki} = \begin{bmatrix} y_k \\ y_i \end{bmatrix}$ and $W_{ki} = \begin{bmatrix} I & W_i \end{bmatrix}$. Then, the projection operator reduces to the affine case but with weights W_{ki}, b_i for input y_{ki} .

B.9 Batch Normalization and Average Pooling

The batch normalization and average pooling layers that appear in the architecture of the residual networks, e.g., ResNet18 applied in this paper, are essentially affine mapping layers whose weights and biases can be extracted accordingly. Therefore, the projection onto the graph of these two layers has a closed-form solution as shown in Eq. (11).

C Implementation Details

C.1 Convergence and Stopping Criterion

The DeepSplit algorithm converges to the optimal solution of the convex problem (6) under mild conditions. Specifically, when J is closed, proper and convex, and when the sets \mathcal{S}_k (convex outer approximations of the graph of the layers) along with \mathcal{X} are closed and convex, we can resort to the convergence results of ADMM [1].

For the LP relaxation (6) of a feed-forward neural network, the primal and dual residuals are defined as

$$\begin{aligned} r_p &= \sum_{k=0}^{\ell-1} \{ \|y_k^+ - x_k^+\|^2 + \|x_{k+1}^+ - z_k^+\|^2 \} \\ r_d &= \rho \sum_{k=1}^{\ell-1} \| (y_k^+ - y_k) + (z_{k-1}^+ - z_{k-1}) \|^2 + \rho (\|y_0^+ - y_0\|_2^2 + \|z_{\ell-1}^+ - z_{\ell-1}\|_2^2). \end{aligned} \quad (22)$$

These are the residuals of the optimality conditions for (6) and converge to zero as the algorithm proceeds. A reasonable termination criterion is that the primal and dual residuals must be small, i.e. $r_p \leq \epsilon_p$ and $r_d \leq \epsilon_d$, where $\epsilon_p > 0$ and $\epsilon_d > 0$ are tolerance levels [1, Chapter 3]. These tolerances can be chosen using an absolute and relative criterion, such as

$$\begin{aligned} \epsilon_p &= \sqrt{p} \epsilon_{abs} + \epsilon_{rel} \max \left\{ (\|x_0\|_2^2 + 2 \sum_{i=1}^{\ell-1} \|x_i\|_2^2 + \|x_\ell\|_2^2)^{\frac{1}{2}} + \left(\sum_{i=0}^{\ell-1} (\|y_i\|_2^2 + \|z_i\|_2^2) \right)^{\frac{1}{2}} \right\} \\ \epsilon_d &= \sqrt{n} \epsilon_{abs} + \epsilon_{rel} (\|\lambda_0\|_2^2 + \sum_{i=1}^{\ell-1} \|\lambda_i + \mu_{i-1}\|_2^2 + \|\mu_{\ell-1}\|_2^2)^{\frac{1}{2}}, \end{aligned}$$

where $p = n_0 + 2 \sum_{i=1}^{\ell-1} n_i + n_\ell$, $n = \sum_{i=0}^{\ell} n_i$, $\epsilon_{abs} > 0$ and $\epsilon_{rel} > 0$ are absolute and relative tolerances. Here n is the dimension of \mathbf{x} , the vector of primal variables that are updated in the first step of the algorithm, and p is the total number of consensus constraints.

For neural networks with general computational graphs such as residual networks, the primal and dual residuals as well as the stopping criteria have different representations from what’s shown above. But with our proposed splitting method, these representations are easy to derive from [1, Chapter 3].

C.2 Parameter Selection

A proper selection of the augmentation constant ρ has a dramatic effect on the convergence of the method. Large values of ρ enforces consensus more quickly, yielding smaller primal residuals but larger dual ones. Conversely, smaller values of ρ leads to larger primal and smaller dual residuals. A commonly used heuristic to make this trade-off is residual balancing [19], in which the penalty parameter varies adaptively based on the following rule:

$$\rho^+ = \begin{cases} \tau\rho & \text{if } r_p > \mu r_d \\ \rho/\tau & \text{if } r_d > \mu r_p \\ \rho & \text{otherwise,} \end{cases}$$

where $\mu, \tau > 1$ are parameters. In our experiments, we found this rule to be effective in speeding up the practical convergence.

C.3 Convolutional Layers

The projection step for affine layers from (11) requires multiplication by the matrix $(I_{n_k} + W_k^\top W_k)^{-1}$ for that layer, where n_k is the number of neurons in the layer. When handling networks with convolutional layers on image data, n_k can easily exceed tens of thousands, so the resulting matrix and its inversion can exceed reasonable memory and computational constraints.

To make the update step practical and in line with typical computational costs of deep convolutional networks, we replace the typical deep learning convolution with an equivalent circular convolution. Specifically, let f_{conv} be a typical strided convolution with padding. We can rewrite f_{conv} as three sequential updates using a circular convolution as $f_{\text{conv}} = f_{\text{post}} \circ f_{\text{circ}} \circ f_{\text{pad}}$, where f_{pad} is a padding step, f_{circ} is a circular convolution, and f_{post} is a post-processing step that performs cropping, downsampling, and adds any bias term from f_{conv} .

We can now treat these three updates as separate, individual layers in our ADMM algorithm. The key observation is that we can use the convolution theorem to implement the ADMM update for the circular convolution f_{circ} efficiently. Specifically, for an input of size $n_k \times n_k$, the projection step from (11) for a circular convolution can be calculated in $O(n_k^2 \log n_k)$ using the fast Fourier transform. We provide the specific details of this procedure in Appendix D.

D FFT Implementation For Circular Convolutions

In order to efficiently implement convolutional layers, recall that we decompose a convolution into the following three steps:

$$f_{\text{conv}} = f_{\text{post}} \circ f_{\text{circ}} \circ f_{\text{pad}} \tag{23}$$

We now discuss in detail how to efficiently perform the (y, z) update for multi-channel, circular convolutions f_{circ} using Fourier transforms. We begin with the single-channel setting, and then extend our procedure to the multi-channel setting. See Appendix B for details regarding the ADMM projection step for f_{pad} and f_{post} .

D.1 Single-channel Circular Convolutions

Let U represent the discrete Fourier transform (DFT) as a linear operator, and let W be the weight matrix for the circular convolution $f_{\text{circ}}(x) = W * x$. Then, using matrix notation, the convolution theorem states that

$$f_{\text{circ}}(x) = W * x = U^*(UW \cdot Ux) = U^*DUx \quad (24)$$

where $D = \text{diag}(UW)$ is a diagonal matrix containing the Fourier transform of W and U^* is the conjugate transpose of U . Then, we can represent the inverse operator from (11) as

$$(I + f_{\text{circ}}^\top f_{\text{circ}})^{-1} = U^*(I + DD)^{-1}U \quad (25)$$

Since $(I + DD)$ is a diagonal matrix, its inverse can be computed quickly by simply inverting the diagonal elements, and requires storage space no larger than the original kernel matrix. Thus, multiplication by the inverse matrix for a circular convolution reduces to two DFTs and an element-wise product. For an input of size $n \times n$, this step has an overall complexity of $O(n^2 \log n)$ when using fast Fourier transforms.

D.2 Multi-channel Circular Convolutions

We now extend the operation for single-channel circular convolutions to multi-channel, which is typically used in convolutional layers found in deep vision classifiers. Specifically, for a circular convolution with n input channels and m output channels, we have

$$f_{\text{circ}}(x)_j = \sum_{i=1}^n W_{ij} * x_i \quad (26)$$

where $f_{\text{circ}}(x)_j$ is the j th output channel output of the circular convolution, W_{ij} is the kernel of the i th input channel for the j th output channel, and x_i is the i th channel of the input x . The convolutional theorem again tells us that

$$f_{\text{circ}}(x)_j = \sum_{i=1}^n U^*D_{ij}Ux_i \quad (27)$$

where $D_{ij} = \text{diag}(UW_{ij})$. This can be re-written more compactly using matrices as

$$f_{\text{circ}}(x) = \bar{U}^* \bar{D} \bar{U} \bar{x} \quad (28)$$

where

- $\bar{U} = \begin{bmatrix} U & \cdots & 0 \\ \vdots & \ddots & \vdots \\ 0 & \cdots & U \end{bmatrix}$ is a block diagonal matrix with n copies of U along the diagonal
- $\bar{U}^* = \begin{bmatrix} U^* & \cdots & 0 \\ \vdots & \ddots & \vdots \\ 0 & \cdots & U^* \end{bmatrix}$ is a block diagonal matrix with m copies of U along the diagonal
- $\bar{D} = \begin{bmatrix} D_{11} & \cdots & D_{n1} \\ \vdots & \ddots & \vdots \\ D_{1m} & \cdots & D_{nm} \end{bmatrix}$ is a block matrix with diagonal blocks where the ij th block is D_{ij}

• $\bar{x} = \begin{bmatrix} x_1 \\ \vdots \\ x_n \end{bmatrix}$ is a vertical stacking of all the input channels.

Then, we can represent the inverse operator from (11) as

$$(I + f_{\text{circ}}^\top f_{\text{circ}})^{-1} = \bar{U}^*(I + \bar{D}\bar{D})^{-1}\bar{U} \quad (29)$$

where $I + \bar{D}\bar{D}$ is a block matrix, where each block is a diagonal matrix. The inverse can then be calculated by the inverting sub-matrices formed from sub-indexing the diagonal components. Specifically, let $\bar{D}_{j::p}$ be a slice of \bar{D} containing elements spaced m elements apart in both column and row directions, starting with the j th item. For example, $\bar{D}_{0::p}$ is the matrix obtained by taking the top-left most element along the diagonal of every block. Then, for $j = 1 \dots m$, we have

$$(I + \bar{D}\bar{D})_{j::p}^{-1} = ((I + \bar{D}\bar{D})_{j::p})^{-1} \quad (30)$$

Thus, calculating this matrix amounts to inverting a batch of p matrices of size $m \times m$. For typical convolutional networks, m is typically well below 1,000, and so this can be calculated quickly. Further note that this only needs to be calculated once as a pre-computation step, and can be reused across different inputs and objectives for the network.

Memory and runtime requirements In practice, we do not store the fully-expanded block diagonal matrices; instead, we omit the zero entries and directly store the the diagonal entries themselves. Consequently, for an input of size p , the diagonal matrices require storage of size $O(mnp)$, and the inverse matrix requires storage of size $O(m^2p)$. Since the discrete Fourier transform can be done in $O(p \log p)$ time with fast Fourier transforms, the overall runtime of the precomputation step to form the matrix inverse is the cost of the initial DFT and the batch matrix inverse, or $O(nmp \log p + m^3p)$. Finally, the runtime of the projection step is $O((n+m)p \log p + n^2mp)$, which is the respective costs of the DFT transformations \bar{U} and \bar{U}^* , as well as the multiplication by \bar{D} . Since the number of channels in a deep network are typically much smaller than the size of the input to a convolution (i.e. $n < p$ and $m < p$), the costs of doing the cyclic convolution with Fourier transforms are in line with typical deep learning architectures.

E Experimental Details

E.1 Architectures, Datasets, and Training Specifics

MNIST We consider two ReLU based architectures. The first one is a fully connected network with layer sizes 784 – 600 – 400 – 200 – 100 – 10 which we denote MNIST-A. It is more than triple the size of that considered by [6] with one additional layer. It is, however, still small enough such that Gurobi is able to solve the LP relaxation, and allows us to compare our running time against Gurobi. The second one is a convolutional network which uses the small convolutional architecture from [38] and consists of two convolutional layers of size 16 – 32 with kernel sizes 4 – 4, strides 2 – 2, and padding 1 – 1. We denote this network by MNIST-B. This architecture is comparable to the convolutional architecture considered by [6], and allows us to compare our running time against the gradient-based SDP solver.

We train both models with an ℓ_∞ PGD adversary at radius $\epsilon = 0.1$, using 7 steps of size $\alpha = 0.02$, with batch size 100 for 100 epochs. We use the Adam optimizer with a cyclic learning rate (maximum learning rate of 0.005), and both models achieve a clean accuracy of 99%.

Table 3: Approximate verification time for solving the LP relaxation through ADMM. Epsilons are evenly spaced within the range.

Model	# of epsilon	Epsilon range	Time (hrs)
MNIST-A	10	[0.01, 0.1]	13.12
MNIST-B	10	[0.01, 0.1]	19.92
CIFAR10	8	[0.5/255, 4/255]	50.69
Bankheist	10	[0.1/255, 1/255]	4.96
Roadrunner	10	[0.1/255, 1/255]	52.33
Pong	10	[0.1/255, 1/255]	31.06

CIFAR10 For CIFAR10, we use the large convolutional architectures from [38], which consists of four convolutional layers with $32 - 32 - 64 - 64$ channels, with strides $1 - 2 - 1 - 2$, kernel sizes $3 - 4 - 3 - 4$, and padding $1 - 1 - 1 - 1$. This is followed by three linear layers of size $512 - 512 - 10$. This is significantly larger than the CIFAR10 architectures considered by [6], and has sufficient capacity to reach 43% adversarial accuracy against an ℓ_∞ PGD adversary at $\epsilon = 8/255$.

The model is trained against a PGD adversary with 7 steps of size $\alpha = 2/255$ at a maximum radius of $\epsilon = 8.8/255$, with batch size 128 for 200 epochs. We used the SGD optimizer with a cyclic learning rate (maximum learning rate of 0.23), momentum 0.9, and weight decay 0.0005. The model achieves a clean test accuracy of 71.8%.

State-robust RL We use the pretrained, adversarially trained, DQNs released by [42] from

https://github.com/chenhongge/SA_DQN

which has not included any license information up to the date of submission of this paper. These models were trained to be robust at $\epsilon = 1/255$ with a PGD adversary for the Atari games Pong, Roadrunner, Freeway, and BankHeist. Each input to the DQN is of size $1 \times 84 \times 84$, which is more than double the size of CIFAR10. The DQN architectures are convolutional networks, with three convolutional layers with $32 - 64 - 64$ channels, with kernel sizes $8 - 4 - 3$, strides $4 - 2 - 1$, and no padding. This is followed by two linear layers of size $512 - K$, where K is the number of discrete actions available in each game.

E.2 Timing Experiments

Runtime summary: We certify the robustness of classifiers for MNIST and CIFAR10 and DQNs in Atari games to ℓ_∞ perturbations over a range of radii. The specific verification setups can be found in Appendix E.3 and E.4. We report the approximate runtime for all experiments in Table 3.

Effects of ADMM parameters: In this subsection, we demonstrate the effects of the algorithm parameters on the convergence of ADMM through two networks: MNIST-A (fully-connected) and MNIST-B (convolutional). Specifically, we focus on the choice of ρ and the application of residual balancing.

We conduct our experiment on the 1938-th example which is randomly chosen from the MNIST test data set. For this example, both MNIST-A and MNIST-B predicts its class (number 4) correctly. We add an ℓ_∞ perturbation of radius $\epsilon = 0.02$ to the input image and verify if the network outputs are robust with respect to class number 3. The maximum number of iterations is restricted to 3000. The objective values, primal and dual residuals of ADMM for MNIST-A and MNIST-B under different augmentation parameters ρ are plotted in Figure 4 and 5, respectively.

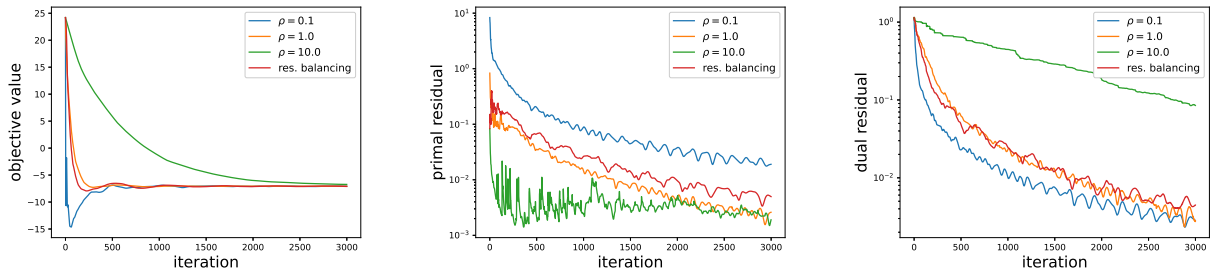


Figure 4: The objective values (left), primal residuals (middle), and dual residuals (right) of ADMM under different augmentation parameters ρ on the MNIST-A (fully-connected) network.

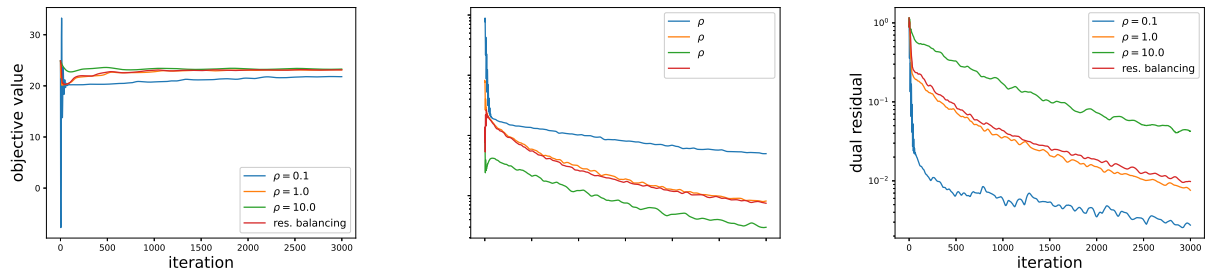


Figure 5: The objective values (left), primal residuals (middle), and dual residuals (right) of ADMM under different augmentation parameters ρ on the MNIST-B (convolutional) network.

The residual balancing in this experiment is applied with initial $\rho = 10.0$, $\tau = 2$, and $\mu = 10$ as described in Section C.2.

The update rule of ADMM suggests that a large value of ρ tends to produce small primal residuals since it puts a large penalty on the violation of the primal feasibility. However, the dual residuals for such ρ tends to be larger. Conversely, a small ρ tends to reduce the dual residuals at the cost of larger primal residuals. This phenomenon is illustrated empirically with the fully-connected network MNIST-A in Figure 4 and the convolutional network MNIST-B in Figure 5.

Since ADMM terminates when both the primal and dual residuals are small enough, in practice we prefer to choose the augmentation parameter ρ not too large or too small in order to balance the reduction in the primal and dual residuals. An effective way to choose a good ρ is residual balancing, which tries to keep the primal and dual residuals close during the ADMM updates by adjusting ρ online. In both Figure 4 and Figure 5, ADMM with residual balancing is initialized with $\rho = 10.0$ and shows significant improvement in convergence rate compared with the case of constant $\rho = 10.0$. As observed in our other experiments, with residual balancing, ADMM becomes insensitive to the initialization of ρ and usually achieves a good convergence rate.

In all of the test accuracy certification results reported in this paper, we initialize $\rho = 1.0$ and apply residual balancing when running ADMM. In different experiments, the stopping criterion parameters $\epsilon_{\text{abs}}, \epsilon_{\text{rel}}$ of ADMM are chosen by trial-and-error to achieve a balance between the accuracy and the running time of the algorithm. Although ADMM has convergence guarantees for its objective values, primal and dual residuals, it may take too many iterations for ADMM to achieve a solution of high accuracy [1].

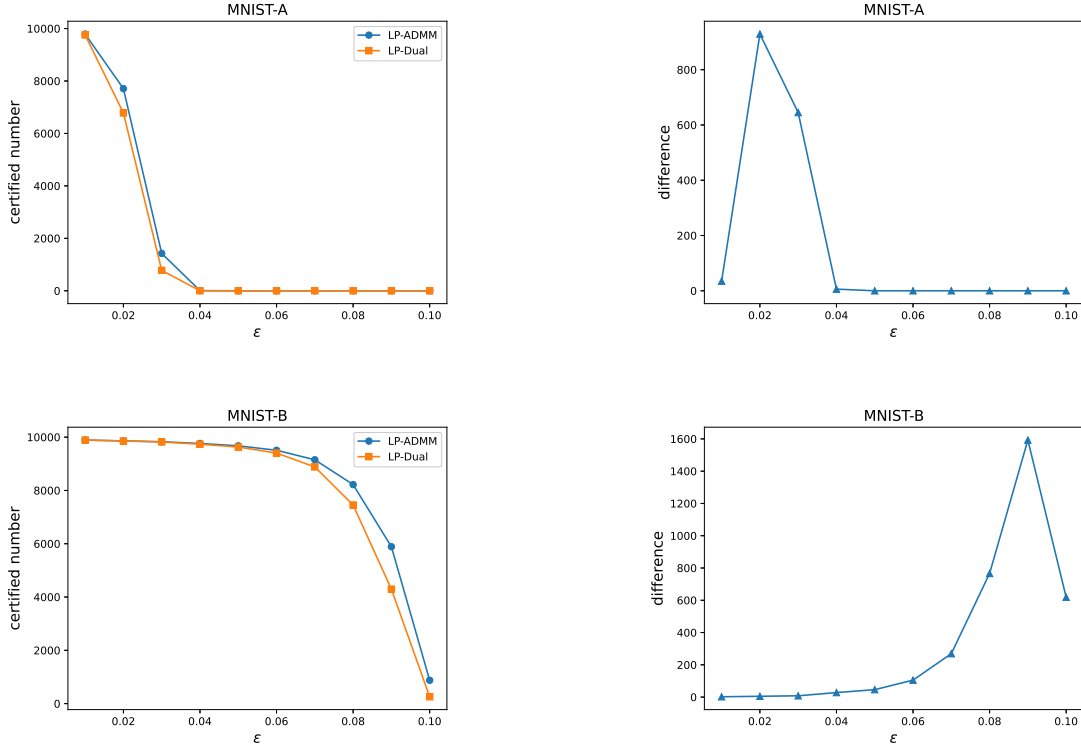


Figure 6: The numbers of certified examples (left column) of ADMM and the linear-based bounds [38,39] for the MNIST-A (upper row) and MNIST-B (lower row) networks and their differences (right column) for each $\epsilon \in \{0.01, 0.02, \dots, 0.10\}$.

E.3 Image Classification

In this section, we report the details of certified test accuracy of our proposed method (ADMM) and the scalable linear-based bounds on LP relaxations (Linear) [38,39] in the image classification tasks of MNIST and CIFAR10.

MNIST: For both the fully-connected network MNIST-A and the convolutional network MNIST-B, we apply LP-ADMM with $\epsilon_{\text{abs}} = 10^{-3}$, $\epsilon_{\text{rel}} = 10^{-3}$ as the stopping criterion, and residual balancing with the initial $\rho = 1.0$. For each classifier network, we go through the 10000 examples in the MNIST test data set and a range of ℓ_∞ perturbation radii ϵ to count the number of certified examples. To make the counting more efficient, we (i) search over ϵ in a descending order since examples that are robust for a larger ϵ are also robust for a smaller ϵ , and (ii) only apply ADMM on examples that cannot be verified by Linear [38,39] since Linear [38,39] gives a more relaxed bound than the LP-relaxation. For each batch of test examples, ADMM solves ten optimization problems of the form (5) with the linear objective function given with respect to each prediction class.

For a range of $\epsilon \in \{0.01, 0.02, \dots, 0.10\}$, the numbers of verified examples of ADMM and Linear [38,39] and their differences are shown in Figure 6 for MNIST-A and MNIST-B, respectively. Exact certified accuracy is reported in Table 4 for a range of ϵ .

CIFAR10: On the CIFAR10 data set, we compare ADMM and Linear [38,39] following the same process as on the MNIST data set. The stopping criterion for LP-ADMM is set as $\epsilon_{\text{abs}} = 10^{-4}$, $\epsilon_{\text{rel}} = 10^{-4}$ and the range of ϵ is set as $\{0.5/255, 1.0/255, \dots, 4.0/255\}$. The numbers of

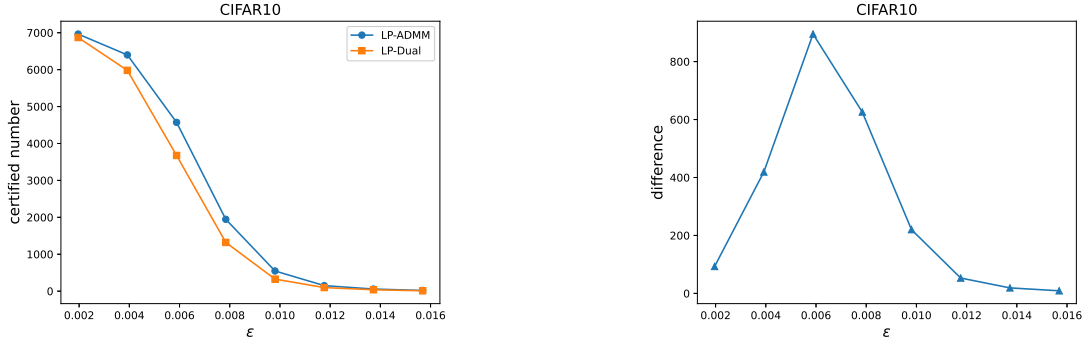


Figure 7: The number of certified examples (left) of ADMM and the linear-based bounds [38, 39] for the CIFAR10 network and their differences (right) for each $\epsilon \in \{0.5/255, 1.0/255, \dots, 4.0/255\}$.

Table 4: Certified accuracy of PGD-trained models on MNIST when using a computationally cheap bound (linear-based bounds [38, 39]) vs. our method (ADMM)

Model	Epsilon	Certified test accuracy (%)		
		Linear [38, 39]	ADMM	Diff
MNIST-A	0.02	67.8	77.1	9.3
	0.03	7.8	14.2	6.5
MNIST-B	0.07	88.8	91.5	2.7
	0.08	74.5	82.2	7.7
	0.09	43.0	58.9	15.9
	0.10	2.6	8.8	6.2

certified examples of ADMM and Linear [38, 39] and their differences are shown in Figure 7.

E.4 Reinforcement Learning

We compare the tightness of ADMM and Linear [38, 39] by verifying the robustness of DQNs on three Atari game benchmarks: BankHeist, Roadrunner, and Pong. The DQNs applied in these experiments are introduced in Appendix E.1.

For each benchmark, we collect 10,000 frames (each with dimension $1 \times 84 \times 84$) across 100 episodes using the natural policy with 100 frames sampled randomly from each episode as the test data set. Note that the input images to the DQNs are already pre-processed such that the pixel values are normalized to $[0, 1]$ with a single channel.

In each game, for each frame in the sampled data set, we verify if the DQN does not change its actions when an ℓ_∞ perturbation of various radii is added to the frame which is the state observation of the agent. The number of actions in BankHeist, Roadrunner and Pong are 6, 6, 4, respectively. Essentially, we reduce the verification of the DQN with finite discrete action space to the same setting as verifying classifiers. Therefore, we apply the same verification process as described in Appendix E.3 with $\epsilon \in \{0.1/255, 0.2/255, \dots, 1.0/255\}$ on all three tasks. The numbers of certified examples of ADMM and Linear [38, 39] and their differences on each task are plotted in Figure 8.

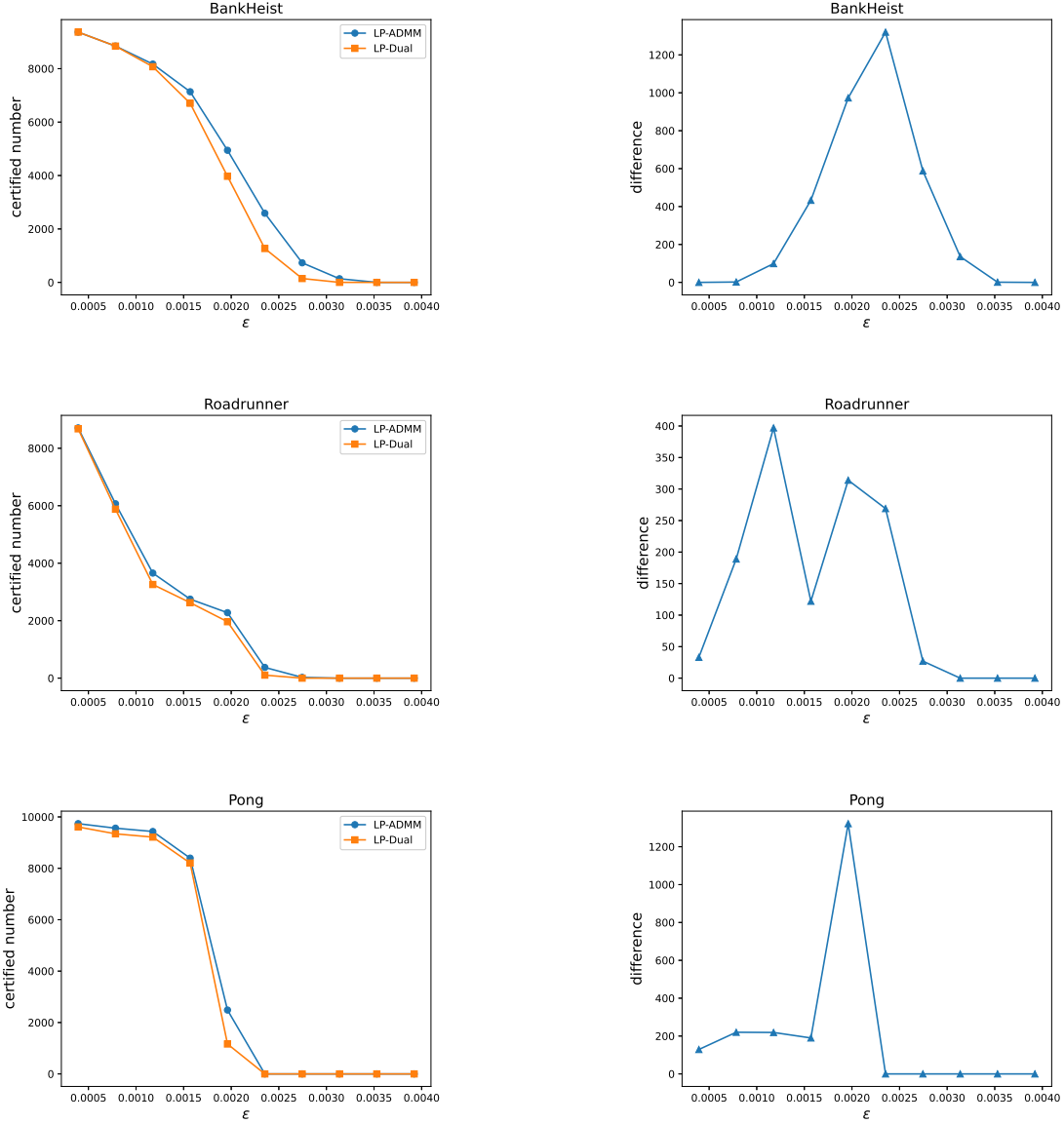


Figure 8: The numbers of certified examples (left column) of ADMM and the linear-based bounds [38,39] and their differences (right column) in the verification of DQNs from the BankHeist (first row), Roadrunner (second row) and Pong (third row) benchmarks. The range of ϵ is given by $\{0.1/255, 0.2/255, \dots, 1.0/255\}$.

F Additional Details on Comparison to Lagrangian-based Methods

In Section 4.1, we compared the certified test accuracy of ADMM with a suite of Lagrangian-based methods [2] on CIFAR10. These Lagrangian-based baselines were implemented using the codes at

<https://github.com/oval-group/decomposition-plnn-bounds>

under the MIT license. As mentioned in Section 3.2, these baselines require solving an inner optimization problem through iterative algorithms. In the experiments of Table 1, the number of iterations of different iterative algorithms are bounded separately such that each Lagrangian-based method listed in Section 4.1 has similar runtime (1 to 10 seconds) to finish verifying one example.

Our ADMM solver averages 9 seconds runtime per example in this verification task, which is of the same level of the runtime of the Lagrangian-based methods, with the stopping criterion of $\epsilon_{abs} = 10^{-4}$, $\epsilon_{rel} = 10^{-3}$ and $\rho = 1.0$.

Architecture size. We note that the architecture we verify in this paper is 10x larger than considered by [3]. However, the released framework could not handle this model size due to their implementation of intermediate bounds. In order to handle this model size, we externally calculated the intermediate bounds (using [38]) and loaded these into the framework for the Lagrangian-based baselines.

G Speed Comparison

Comparison with LP solver: To demonstrate the effectiveness of GPU-acceleration in the DeepSplit algorithm, we compare the runtime of DeepSplit and Gurobi in solving LP relaxations that bound the output range of MNIST-A network (the fully connected network defined in Appendix E.1) with ℓ_∞ perturbations in the input. Specifically, for a given example in the MNIST test data set, we apply DeepSplit/Gurobi layer-by-layer to find the tightest pre-activation bounds under the LP-relaxation.

Recall that the MNIST-A network is a fully-connected network with architecture 784 – 600 – 400 – 200 – 100 – 10. With the Gurobi solver, we need to solve 2×600 LPs sequentially to obtain the lower and upper bounds for the first activation layer, 2×400 LPs for the second activation layer, and so forth. With DeepSplit, the pre-activation bounds can be computed in batch and allows GPU-acceleration.

In our experiment, we fix the radius of the ℓ_∞ perturbation at the input image as $\epsilon = 0.02$. For the Gurobi solver, we randomly choose 10 samples from the test data set and compute the pre-activation bounds layer-by-layer. The LP relaxation is formulated in CVXPY and solved by Gurobi v9.1 on an Intel Core i7-6700K CPU. For each example, the total solver time of Gurobi is recorded with the average solver time being 275.9 seconds. For the DeepSplit method, we compute the pre-activation bounds layer-by-layer on 19 randomly chosen examples. The algorithm applies residual balancing with the initial $\rho = 1.0$ and the stopping criterion is given by $\epsilon_{abs} = 10^{-4}$, $\epsilon_{rel} = 10^{-3}$. The total running time of DeepSplit is 717.9 seconds, with 37.8 seconds per example on average. With the GPU-acceleration, our method achieves 7x speedup in verifying NN properties compared with the commercial-grade Gurobi solver.

Comparison with SDP solver: Our method is significantly faster than solving the convex relaxation through other approaches. For example, it took our method approximately 20 hours to verify all MNIST test set images for the convolutional architecture at 10 different epsilon values

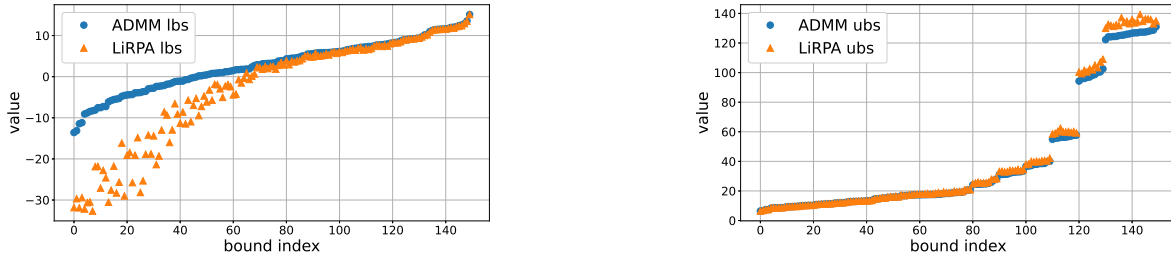


Figure 9: ResNet18 output lower (left) and upper (right) bounds obtained using either ADMM (blue dots) and LiRPA (orange triangles) from the first 15 CIFAR10 test examples. Higher lower bounds and lower upper bounds are better. For ease of visualization, bounds are sorted in ascending order according to the ADMM bound.

(See Table 3), taking on average 2 hours per epsilon to verify all 10,000 examples. See E.2 for the running time summary of each experiment. In contrast, the SDP relaxation [27] takes 3 hours to verify 500 examples at one epsilon value for a similarly sized CNN. This highlights the difference in speed and scalability of solving the LP relaxation over the SDP one, albeit at the cost of looser verification guarantees.

H Scalability

To highlight the scalability of our approach, we consider a ResNet18 network trained on CIFAR10 whose max pooling layer is replaced by a down-sampling convolutional layer for comparison with LiRPA [39]³ (codes available at

https://github.com/KaidiXu/auto_LiRPA

under the BSD 3-Clause "New" or "Revised" license), which is capable of computing provable linear bounds for the outputs of general neural networks and is the only method available so far that can handle ResNet18. The ResNet18 is adversarially trained using the fast adversarial training code from [37].

In our experiments, for the first 15 test examples in CIFAR10, we use LiRPA to compute the preactivation bounds for each ReLU layer in ResNet18 and then apply ADMM to compute the lower and upper bounds of ResNet18 outputs (there are 10 outputs corresponding to the 10 classes of the dataset). The ADMM is run with stopping criterion $\epsilon_{abs} = 10^{-5}$, $\epsilon_{rel} = 10^{-4}$ and augmentation parameter $\rho = 1.0$. With $\epsilon = 1/255$, the lower/upper bounds of ADMM from these 15 examples are arranged in an ascending order in Figure 9 and are compared with those obtained by LiRPA. We observe that the bounds from ADMM are consistently tighter than those from LiRPA. In Figure 2, we truncate the smallest/largest 50 lower/upper bounds to give a more clear demonstration the differences between these two methods. The average running time of ADMM across the 15 examples is 2202 seconds.

³The max pooling layer has not been considered in the implementation of LiRPA by the submission of this paper.